Springer

Journal of
Mechanical
Science and
Technology

Journal of Mechanical Science and Technology 23 (2009) 1765~1772

www.springerlink.com/content/1738-494x
DOI 10.1007/s12206-009-0601-3

# Numerical study of droplet dynamics in a PEMFC gas channel with multiple pores †

Jiyoung Choi and Gihun Son*

*Department of Mechanical Engineering, Sogang University, Seoul, 121-742, Korea*

(Manuscript Received March 4, 2009; Revised March 18, 2009; Accepted March 18, 2009)

**Abstract**

The water droplet motion in a PEMFC gas channel with multiple pores, through which water emerges, is studied numerically by solving the equations governing the conservation of mass and momentum. The liquid-gas interface is tracked by a level set method which is based on a sharp-interface representation for accurately imposing the matching conditions at the interface. The method is modified to implement the contact angle conditions on the walls and pores. The dynamic interaction between the droplets growing on multiple pores is investigated by conducting the computations until the droplet growth and sliding motion exhibits a periodic pattern. The numerical results show that the configuration subject to droplet merging is not effective for water removal and that the wettability of channel wall strongly affects water management in the PEMFC gas channel.

*Keywords*: Contact angle; Droplet dynamics; Level set method; PEMFC gas channel

## 1. Introduction

In a proton exchange membrane fuel cell (PEMFC), electricity is generated by the electrochemical reaction of hydrogen and oxygen. As a by-product, liquid water forms at the cathode side of a membrane electrode assembly (MEA) where oxygen is provided from the air (or gas) channel through the porous gas diffusion layer (GDL). The flow passages for oxygen supply are also used for the transport of liquid water. When the water is not removed properly, it may block (or flood) the oxygen supply passages including the pores of the GDL and the air channel, as observed experimentally by Zhang et al. [1]. The water management is essentially important for the performance of a PEMFC, which was reviewed in detail by Kandlikar [2]. In this study, we focus on the water transport in a PEMFC air channel including the GDL surface. Despite a number of studies, the dynamics of water droplets emerging from the GDL surface is still not well understood.

Recently, numerical simulations have been performed for further clarifying the droplet dynamics. Mukherjee and Kandlikar [3] simulated a growing water droplet in an air supply channel with 1 mm square section using the level set (LS) method, in which the liquid-gas interface is tracked by the LS function that is defined as a signed distance from the interface. The smooth LS function can be used to compute an interface curvature accurately. They investigated the effects of inlet air velocity and contact angle on the droplet growth and detachment, but their prediction of droplet detachment diameter was much smaller than the experimental data available in the literature [2]. Subsequently, Zhu et al. [4] performed a more comprehensive numerical simulation of droplet emerging through a pore into an air flow channel with 0.25 mm square cross section. Using the volume-of-fluid (VOF) method, in which the liquid-gas interface is tracked by the VOF function

† This paper was presented at the 7th JSME-KSME Thermal and Fluids Engineering Conference, Sapporo, Japan, October 2008.

*Corresponding author. Tel.: +82 32 872 309682 2 705 8641, Fax.: +82 32 868 171682 2 712 0799
E-mail address: kykim@inha.ac.krgihun@sogang.ac.kr

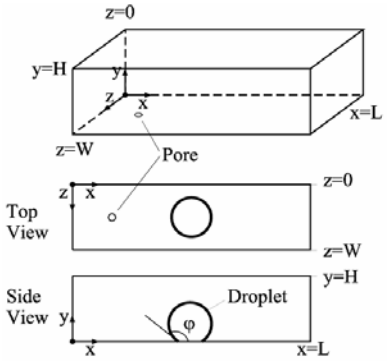


Fig. 1. Computational domain.

representing the volume fraction of a particular phase in each cell, they quantified the effects of contact angle, inlet air velocity, emerging water velocity and pore size on the droplet removal process.

In actual operation of a PEMFC, droplets appear simultaneously through multiple pores of the channel [1]. As the number of droplets increases with electricity generation, the droplets interact with each other and merge frequently. A fundamental understanding of the droplet interaction is very important for solving the water accumulation problem, which is one of the key issues in designing of a PEMFC. However, few studies for the phenomena are reported in the literature.

In this study, numerical simulations are performed to investigate the dynamic interaction between the droplets growing on multiple pores. The droplet shape is determined by the level set (LS) method which is modified to treat the contact angle conditions on the wall and pores. The matching conditions at the interface are accurately imposed by incorporating the ghost fluid approach based on a sharp-interface representation. The effects of inlet air velocity, droplet merger and contact angle on droplet motion and water removal are quantified.

## 2. Numerical analysis

The present numerical approach is based on the LS formulation developed by Choi and Son [5] for computation of droplet motion in a microchannel. The method is extended for numerical simulation of droplet growth and sliding motion in a PEMFC gas channel. The liquid-gas interface is tracked by the LS function $\phi$, which is defined as a signed distance from the interface. The negative sign is chosen for the gas phase and the positive sign for the liquid phase.

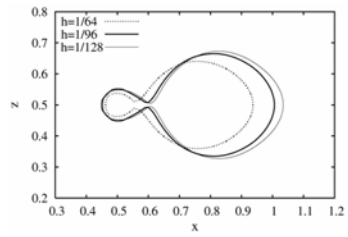


(a)

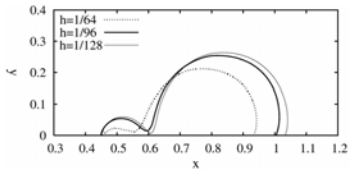


(b)

Fig. 2. Droplet shape at detachment from a pore at the cross-section of (a) y=0 and (b) z=0.5.

The equations governing the conse —rvation of mass and momentum for the liquid-gas region can be written as

$$\nabla \cdot \mathbf{u} = 0 \tag{1}$$

$$\rho \frac{D\mathbf{u}}{Dt} = -\nabla p + \rho \mathbf{g} - \sigma \kappa \nabla \alpha + \nabla \cdot \mu [\nabla \mathbf{u} + (\nabla \mathbf{u})^T] \tag{2}$$

where

$$\frac{D}{Dt} = \frac{\partial}{\partial t} + \mathbf{u} \cdot \nabla$$

$$\kappa = \nabla \cdot (\nabla \phi / |\nabla \phi|)$$

$$\alpha = 1 \quad \text{if } \phi > 0$$

$$= 0 \quad \text{if } \phi \le 0$$

$$\rho = \rho_g (1 - F_\phi) + \rho_l F_\phi$$

$$\mu^{-1} = \mu_g^{-1} (1 - F_\phi) + \mu_l^{-1} F_\phi$$

Here, $\alpha$ is the discontinuous step function and the interface curvature $\kappa$ is evaluated by the smooth LS function. The effective density $\rho$ and viscosi- ty $\mu$ are evaluated from a fraction function $F_\phi$, which is described in [5]. In the level set formulation, the LS function $\phi$ is advanced and reinitialized as

$$\frac{\partial \phi}{\partial t} + \mathbf{u} \cdot \nabla \phi = 0 \tag{3}$$

$$\frac{\partial \phi}{\partial \tau} = S(\phi)(1 - |\nabla \phi|) \tag{4}$$

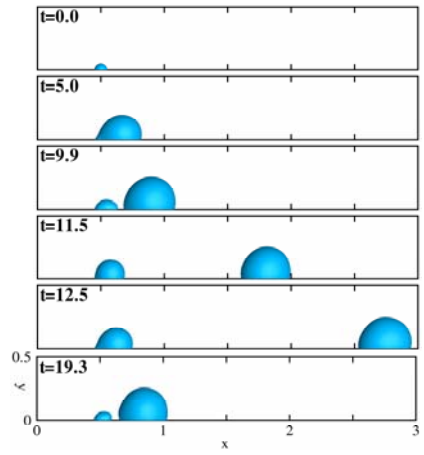


(a)

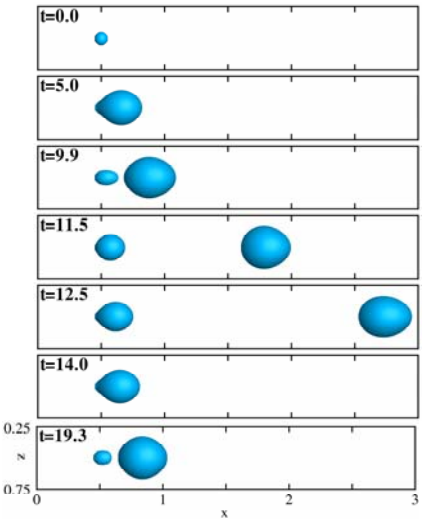


(b)

Fig. 3. Droplet growth and sliding pattern for $N_{pore}$=1, $u_a$=3 and $v_w$=0.25: (a) side view and (b) top view.

where

$$S(\phi) = 0 \quad \text{if } |\phi| \le h/2$$
$$= \frac{\phi}{\sqrt{\phi^2 + h^2}} \quad \text{otherwise} \tag{5}$$

Here $h$ is a grid spacing. This formulation of the sign function improves the mass-conservation property of LS method significantly.

The boundary conditions used in this study are as follows (refer to Fig. 1):

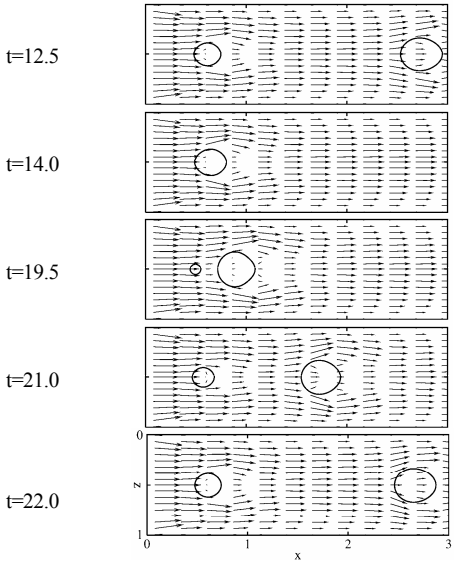


Fig. 4. Velocity field at y=0.1 for $N_{pore}$=1, $u_a$=3 and $v_w$=0.25.

at the inlet ( $x = 0$),

$$u = u_a, \quad v = w = 0, \quad \frac{\partial \phi}{\partial x} = 0 \tag{6}$$

at the outlet ( $x = L$ ),

$$p = 0, \quad \frac{\partial \mathbf{u}}{\partial x} = \frac{\partial \phi}{\partial x} = 0 \tag{7}$$

at the wall ( $y$ =0, H and $z$ =0, W ),

$$\mathbf{u} = 0, \quad \mathbf{n}_w \cdot \nabla \phi = \cos\varphi \tag{8}$$

In Eq. (8), a contact angle $\varphi$, formed on the liquid-gas-solid interline (or contact line), is used to evaluate the LS function at the wall. Assuming that the pore is occupied by the liquid all the time, an additional constraint, $\phi \ge 0$, is imposed for evaluation of the LS function at the pores of the bottom wall, $y = 0$. An inflow condition for the emerging water, $v = v_w$ is also imposed at the pores.

## 3. Results and discussion

The computations are performed for water droplet motion in a microchannel with pores. The effect of gravity is neglected in this analysis. In presenting numerical results including figures, lengths are scaled by 1 mm, velocities by 1 m/s, and time by 1 ms. The

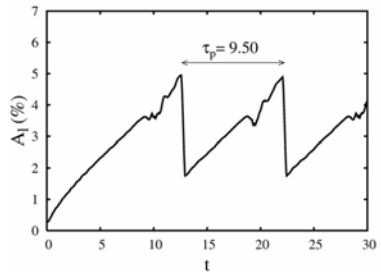


(a)

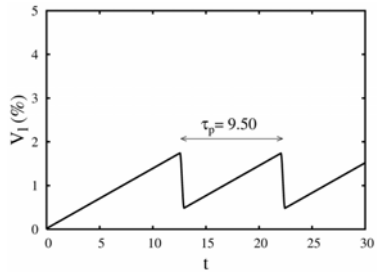


(b)

Fig. 5. Time variation of the liquid fraction for $N_{pore}$=1, $u_a$=3 and $v_w$=0.25: (a) liquid area fraction $A_l$ and (b) liquid volume fraction $V_l$.

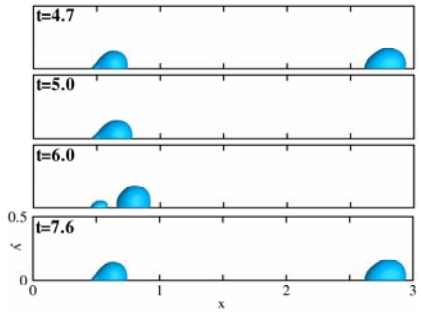


(a)

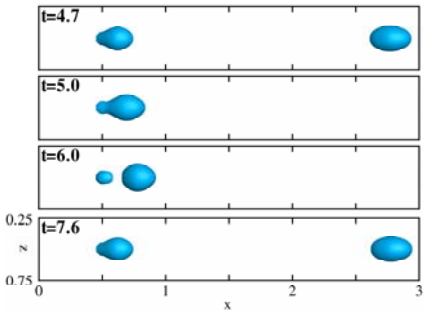


(b)

Fig. 6. Droplet growth and sliding pattern for $N_{pore}$=1, $u_a$=5 and $v_w$=0.25: (a) side view and (b) top view.

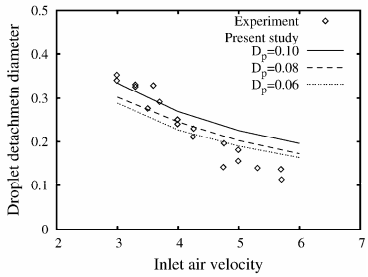


Fig. 7. Effects of air velocity and pore size on droplet detachment diameter for $N_{pore}$=1 and $v_w$=0.25.

computational domain is chosen to be a rectangular channel as depicted in Fig. 1. The channel has a cross-section of $1\times0.5$, which is the same with the experiment of Zhang et al. [1], and a length of 3. As the base case, we choose an inlet air velocity of $u_a$=3, a water injection velocity of $v_w$=0.25, a pore diameter of $D_p$=0.1 and the location of a pore of x=0.5 and z=0.5. The contact angle of the bottom wall is set to $110^o$ and the other walls to $40^o$.

First, for grid resolution test we use three different grid spacings of h=1/64, h=1/96 and h=1/128. The results are plotted in Fig. 2. In each case, the liquid-gas interface (or droplet shape) was obtained just before the growing droplet detaches from a pore. The difference of the interfaces between successive mesh sizes is seen to get smaller when the grid spacing decreases. When the droplet detaches from a pore, its diameters of the droplet are 0.287, 0.335, and 0.348, respectively. The difference between the finest grids is 3.7%. Therefore the present computations are conducted with h=1/96 to save the computing time without losing the accuracy of numerical results. In the following sections, we first present the droplet dynamics on a single pore and then the interaction between two pores. The number of pores is denoted by $N_{pore}$.

### *3.1 Droplet dynamics on a single pore*

Fig. 3 presents the time evolution of the droplet growth (or water removal) pattern for the base case with a single pore. Initially, a hemispherical water droplet with a diameter of pore size is placed on the bottom wall as demonstrated at t=0. The water droplet fed through the pore with $v_w$=0.25 grows up in the air channel until it is detached from the pore by the air flow at t=9.9. The detached droplet has a diameter $D_d$ of 0.335, where the diameter is evaluated by assuming the droplet to be a sphere. It slides along the air

Table 1. Comparison of characteristic variables.

| $N_{pore}$ | pore arrangement | $\varphi_s$ | $D_d$ | $A_{l,av}$ (%) | $V_{l,av}$ (%) | $\tau_p$ |
|---|---|---|---|---|---|---|
| 1 | - | 110° | 0.335 | 3.22 | 1.11 | 9.50 |
| 2 | case1 $d_p$=0.5 | 110° | 0.304 | 5.63 | 1.77 | 7.10 |
| 2 | case2 $d_p$=0.2 | 110° | 0.442 | 5.60 | 2.39 | 10.87 |
| 2 | case3 $d_p$=0.5 | 110° | 0.417 | 5.32 | 2.05 | 10.03 |
| 2 | near sidewall | 40° | 0.630 | 8.10 | 6.85 | 31.8 |
| 2 | near sidewall | 110° | 0.477 | 7.77 | 3.11 | 13.8 |

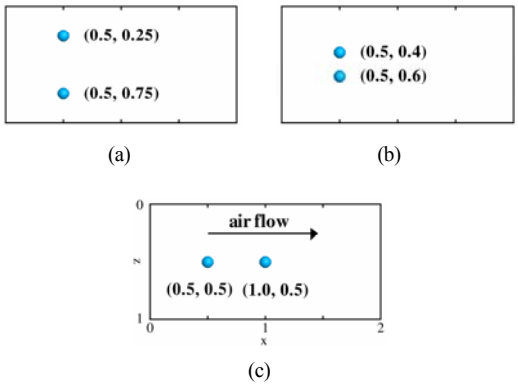


(a) (b)

(c)

Fig. 8. Two-pore arrangement for computations of droplet interaction: (a) case 1 with $d_p$=0.5, (b) case 2 with $d_p$ =0.2 and (c) case 3 with $d_p$ =0.5.

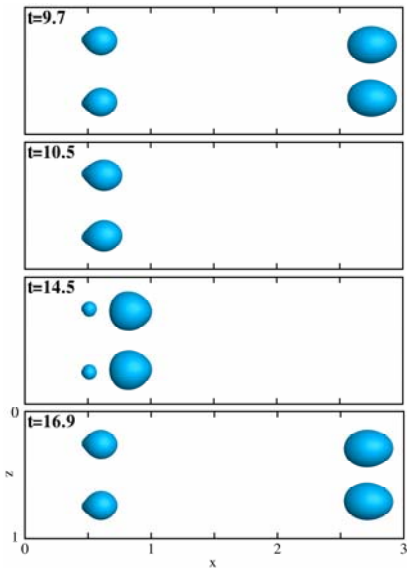


Fig. 9. Droplet growth and sliding pattern for case 1 with two-pore arrangement perpendicular to air flow and $d_p$ =0.5.

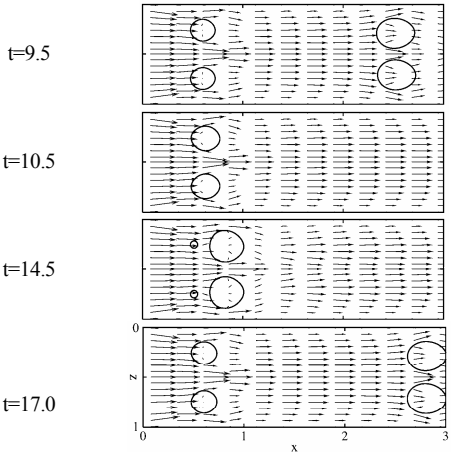


Fig. 10. Velocity field at y=0.1 for case 1 with two-pore arrangement perpendicular to air flow and $d_p$ =0.5.

channel satisfying the contact angle at the bottom wall, $\varphi_b$=110°, while a new droplet emerges through the pore, and then at t=12.5, the droplet arrives at the outlet. Thereafter, the droplet growth, detachment and slide process is repeated all over again, as seen for the period of $9.9 \le t \le 19.3$. The velocity field associated with the droplet motion is plotted in Fig. 4. The air flow around the pore located at (x,z)=(0.5, 0.5) is distorted by a growing droplet. As the velocity gradient becomes steeper with the droplet growth, the drag force acting on the droplet increases and then induces the droplet to detach from the pore. It is also observed that the detached droplet changes the air velocity field during its sliding along the channel, but its influence is limited near the sliding droplet and does not appear around a new growing droplet. Fig. 5 shows the time variation of $A_l$ and $V_l$ during several cycles of droplet growth and sliding. Here, $A_l$ is the area portion occupied by the liquid on the bottom wall and $V_l$ is the ratio of liquid volume to total channel volume. The liquid fractions are measures of water accumulation which prevents the supply of oxygen to the reacting site. $A_l$ and $V_l$ increase gradually as the droplet grows on a pore through which water emerges, and then they drop rapidly while the detached droplet moves out of the channel at x=3. Thereafter, the variations for $A_l$ and $V_l$ are repeated with a period $\tau_p$ of 9.50. When averaged over the period, $A_{l,av}$ is 3.22% and $V_{l,av}$ is 1.11%, as listed in Table 1.

When the inlet air velocity is increased to $u_a$=5, the droplet growth and sliding process occurs as plotted in the Fig. 6. Compared with Fig. 3 for $u_a$=3, the detached droplet becomes much smaller, $D_d$=0.226,

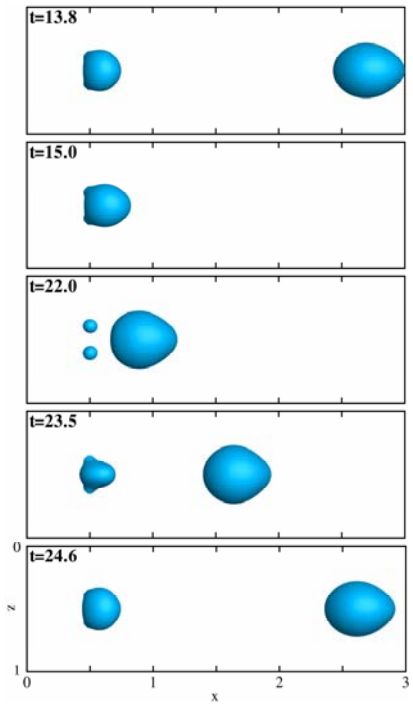


Fig. 11. Droplet growth and sliding pattern for case 2 with two-pore arrangement perpendicular to air flow and $d_p$ =0.2.

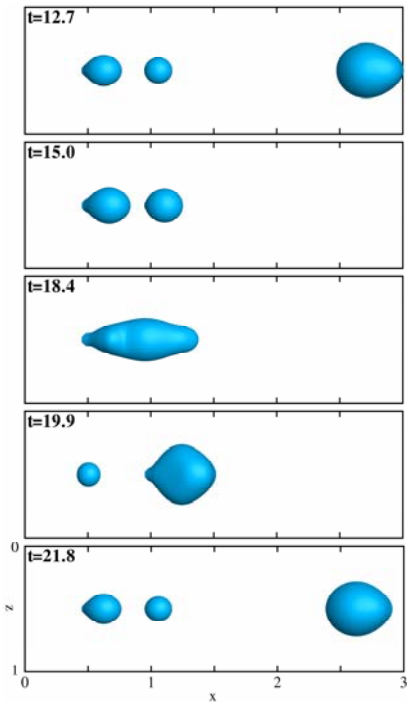


Fig. 12. Droplet growth and sliding pattern for case 3 with two-pore arrangement parallel to air flow and $d_p$ =0.5.

and the process period $\tau_p$ shrinks up to 2.93 as the drag force acting on a droplet is increased with air velocity. Also, the liquid fractions $A_{l,av}$ and $V_{l,av}$ are decreased by 64% and 43%, respectively. This indicates the air velocity is one of the important parameters determining the water removal rate. Fig. 7 presents the effects of inlet air velocity and pore size on the droplet detachment diameter. The diameter decreases as the air velocity increases and the pore size decreases. The experimental data of Zhang et al. [1], which was obtained on a Toray carbon paper GDL surface with $\varphi_b$=110°, are also included in the figure. The numerical prediction obtained in the present study is found to be comparable to the experimental data except that the dependence of detachment diameter on inlet air velocity is slightly weaker in the numerical prediction.

### *3.2 Interaction between two droplets*

The computations are further carried out to investigate the dynamic interaction between the droplets growing on two pores. We consider three configurations of pores depicted in Fig. 8 while keeping $u_a$=3 and $v_w$=0.25.

Fig. 9 shows the droplet motion for case 1 with $d_p$=0.5. Two droplets are observed to grow and slide independently. However, compared with the single pore case, the droplet detaches earlier and its diameter is decreased by 9.3% (refer to Table 1). The earlier detachment is caused by fact that the air velocity passing around the droplets increases as the flow cross section of the channel is reduced with the number of droplets, which is seen from the comparison of Figs. 4 and 10. In this two-pore arrangement, $A_{l,av}$ and $V_{l,av}$ are 75% and 60% larger than the single pore case, as compared in Table 1. The increase in $A_{l,av}$ and $V_{l,av}$ is relatively small if considering the emerging water rate is twice the single pore case while keeping $v_w$=0.25.

When the distance between the pores, $d_p$, is decreased to 0.2, the droplet motion changes as plotted in Fig. 11. The droplets growing on two pores merge in the z direction and are developed into a large droplet. The large merged droplet is fed from two pores before it is separated from the pores. The detached droplet slides along the air channel while a new cycle of droplet growth and merger is repeated near the pores. The droplet detachment diameter $D_d$ is increased by 45.4% compared with case 1. This large

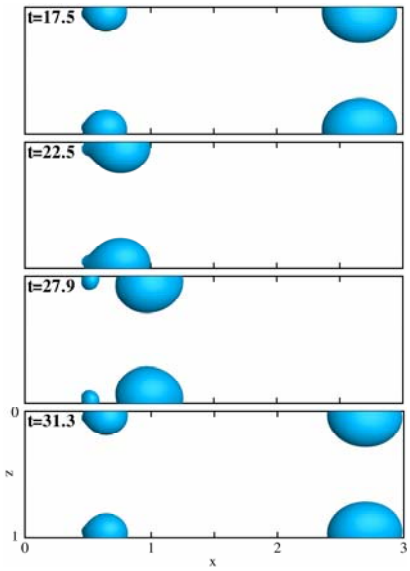


Fig. 13. Droplet motion near the sidewall for $N_{pore}$=2, $u_a$=3 and $v_w$=0.25 and $\varphi_s$=110°.

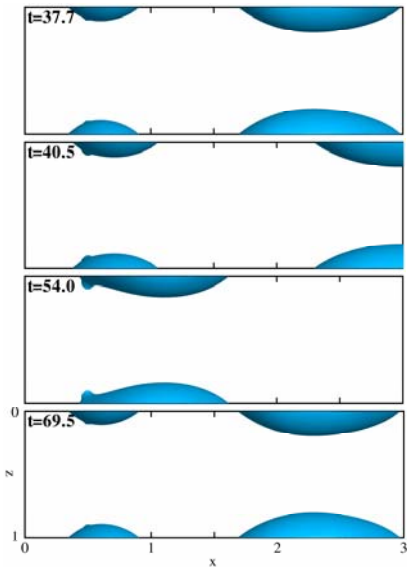


Fig. 14. Droplet motion near the sidewall for $N_{pore}$=2, $u_a$=3 and $v_w$=0.25 and $\varphi_s$=40°.

increase of $D_d$ is caused by the strong surface tension force holding the droplet to the two pores. Fig. 12 presents the droplet motion for case 3, in which two-pore arrangement is parallel to the air flow with $d_p$=0.5. The droplets growing on the pores merges in the x direction. The elongated portion of the merged droplet springs back quickly due to the restoring force of surface tension. Thereafter the droplet detaches from the pores in sequence. $D_d$ is increased by 37% in comparison to case 1 without droplet merger.

A periodic sequence of droplet growth and sliding is observed to occur in all the cases. The process period become larger in case 2 and case 3 where the droplet merger occurs. The liquid fractions $A_{l,av}$ and $V_{l,av}$ averaged over the period are listed in Table 1. The comparison shows that the existence of droplet merger significantly increases the liquid volume fraction, $V_{l,av}$, whereas it slightly reduces the liquid area on the bottom wall, $A_{l,av}$. This means that the pore arrangement subject to droplet merger is not effective for water removal.

The computations are also performed to investigate the droplet motion when droplets touch the sidewall as well as the bottom wall, which will occur more frequently when the number of pores increases. For this case, two pores are placed at (x,z)=(0.5, 0.05) and (0.5, 0.95), respectively. The contact angle $\varphi_s$ at the sidewall is varied while keeping the contact angle of the bottom wall constant as 110°. Fig. 13 shows the result for $\varphi_s$=110°. While the droplet grows and slides, it contacts the bottom and side walls all the time. The droplet detaches from the pore at $D_d$=0.477, which is much larger than for the droplet in contact with only the bottom wall. The droplet growth and sliding period is also significantly increased as listed in Table 1. When the sidewall contact angle is reduced to 40°, the droplet motion occurs as plotted in Fig. 14. The droplet is observed to spread widely along the hydrophilic sidewall, where the flow directional component of surface tension force acting on the liquid-gas-solid interline becomes large. As the droplet spreads up the sidewall with a lower contact angle, the contact area between the droplet and the bottom wall decreases. This observation can lead to an argument that the combination of a hydrophilic sidewall and a hydrophobic bottom wall is an effective way for the removal of water droplets from the bottom wall, as proposed by Cai et al. [6]. However, the present computation for the droplet motion with $\varphi_s$=40°, which is carried out over several cycles, shows that the droplet detachment diameter is increased by 59% compared with $\varphi_s$=110° and the detached droplet slides very slowly on the hydrophilic sidewall as the droplet-wall contact area increases. The cycle period of water transport process is much larger in the case of $\varphi_s$=40°. The liquid fractions $A_{l,av}$ and $V_{l,av}$ averaged over the period are listed in Table 1. Compared with the results for $\varphi_s$=40°, $A_{l,av}$ and $V_{l,av}$ for $\varphi_s$=110° are reduced

by 4% and 55%, respectively. This result indicates that a hydrophobic sidewall is more effective for water removal.

## 4. Conclusions

The water droplet motion in a PEMFC air channel with pores is investigated numerically by employing the level set method, which is improved to accurately impose the matching conditions at the interface by incorporating a sharp-interface approach and is modified to treat the contact angles on the walls and pores.

The main conclusions are:

1. The droplet diameter at detachment from a pore decreases as the air velocity increases and the pore size decreases. The numerical prediction obtained in the present study is comparable to the experimental data available in the literature.

2. The droplet detachment diameter is reduced with increasing the number of pores as long as the interaction between droplets is weak. When the droplets merge, however, the volume fraction occupied by the water is increased significantly. This indicates that the pore arrangement subject to droplet merger is not effective for water removal in a PEFMFC gas channel.

3. When the droplet contacts the sidewall as well as the bottom wall, the droplet transport process becomes slow. The water accumulation is pronounced on the hydrophilic sidewall where the droplet contact area is expanded easily.

## Acknowledgment

This work was supported by the Sogang University Research Grant of 2008.

## References

[1] F. Y. Zhang, X. G. Yang and C. Y. Wang, Liquid water removal from a polymer electrolyte fuel cell, *J. Electrochem. Soc*., 153 (2006) A225-A232.

[2] S. G. Kandlikar, Microscale and macroscale aspects of water management challenge in pem fuel cells, *Heat Transfer Engineering*, 29 (2008) 575-587.

[3] A. Mukherkee and S. G. Kandlikar, A numerical analysis of growing water droplet inside an air supply channel of a PEM fuel cell, *Proc. 2006 ASME International Mechanical Engineering Congress and Exposition*, Chicago, IMECE 2006-14807.

[4] X. Zhu, P. C. Sui and N. Djilali, Three-dimensional numerical simulations of water droplet dynamics in a pem gas channel, *J. Power Sources*, 181 (2008) 101-115.

[5] J. Choi and G. Son, Numerical study of droplet motion in a microchannel with different contact angles, *J. Mechanical Science and Technology*, 22 (2008) 2590-2599.

[6] Y. H. Cai, J. Hu, H. P. Ma, B. L. Ui and H. M. Zhang, Effects of hydrophilic/ hydrophobic properties on the water behavior in the micro-channels of a proton exchange membrane fuel cell, *J. Power Sources*, 161 (2006) 843-848.

**Gihun Son** received his B.S. and M.S. degrees in Mechanical Engineering from Seoul National University in 1986 and 1988, respectively, and Ph.D. degree in Mechanical Engineering from UCLA in 1996. Dr. Son is currently a professor of Mechanical Engineering at Sogang University in Seoul, Korea. His research interests are in the area of multiphase dynamics, heat transfer, and power system simulation.

**Jiyoung Choi** received a B.S. degree in Mechanical Engineering from Sogang University in 2005. He is a graduate student of Mechanical Engineering at Sogang University in Seoul, Korea. Choi's research interests are in the area of PEM fuel cell and microfluidics.